DESIGN AND TESTING OF MESOSCALE MODELS OF INDUSTRIAL SURFACTANTS BY DISSIPATIVE PARTICLE DYNAMICS

By

RUNFANG MAO

A thesis submitted to the

Graduate School – New Brunswick

Rutgers, The State University of New Jersey

In partial fulfillment of the requirement

For the degree of

Master of Science

Graduate Program in Chemical and Biochemical Engineering

Written under the direction of

Dr. Alexander V. Neimark

Dr. Aleksey Vishnyakov

And approved by

_____

_____

_____

_____

New Brunswick, New Jersey

January, 2016

ABSTRACT OF THE THESIS

DESIGN AND TESTING OF MESOSCALE MODELS OF INDUSTRIAL SURFACTANTS BY DISSIPATIVE PARTICLE DYNAMICS

By RUNFANG MAO

Thesis Director:

Dr. Alexander V. Neimark

Dr. Aleksey Vishnyakov

Dissipative particle dynamics simulation with novel model is applied to predict aggregation in ionic surfactants. Anionic surfactant sodium dodecyl sulfate (SDS) and cationic surfactant cetyl trimethyl ammonium bromide (CTAB) are chosen as characteristic examples. Coarse-grained models are constructed from infinite dilution activity coefficient in reference solutions and atomistic simulations. Ionic groups are modeled as beads with charges distributed around the bead centers and placed in implicit dielectric medium. The model of ionic surfactant semi-quantitatively reproduces the dependence of self-assembly in solutions of CTAB and SDS on surfactant concentration, the molarity of added electrolyte. In particular, the decline of the free surfactant concentration with increasing total surfactant loading, as well as the aggregation transition in single-component surfactant cause by salt addition are predicted correctly. Addition of CTAB to a micellar solution of SDS causes a transition to worm-like micelles and then to mini-vesicles. This systematic methodology has been further extended to carbopol system. A stable carbopol film has been observed after equilibrium based on this model. Further investigation to

study rheology of surfactant-carbopol system are required in future work, like add surfactant into this system.

ACKNOWLEDGEMENTS

First and foremost, I would like to express my deepest gratitude to my advisors, Prof. Alexander V. Neimark and Dr. Aleksey Vishnvakov, whose encouragement, insightful guidance and great support during my M.S. study helped me to complete my research project. It is my honor to have the opportunity to study molecular simulation in their group. I believe that everything that I learned here today will benefit my life in the future.

I am also heartily thankful to Dr. Ming-Tsung Lee. He guided me and gave insightful suggestions about coding, algorithm and technical details for the simulation. This research would not have been possible without his invaluable advice, support and their enormous patience throughout my time at Rutgers University.

Furthermore, I would like to thank Prof. Yee Chiew for being my committee member and providing invaluable advice on my work.

Finally, I take this opportunity to convey my sincere thanks to my dear boyfriend Jierui Liang, our loving parents, my group members, and all of my friends who supported me in any respect during my M.S study.

Part of this work is published in The Journal of Physical Chemistry B. Reprinted (adapted) with permission from ("Modelling aggregation of Ionic Surfactants Using a Smearing Charge Approximation in Dissipative Particle Dynamics Simulation", The Journal of Physical Chemistry B) [1] Copyright (2015) American Chemical Society.

TABLE OF CONTENTS

List of Tables

List of Illustration

Chapter 1 Introduction

Self-assembly of surfactant is a ubiquitous phenomenon and important in various areas ranging from living systems to non-living systems. Understanding the principle and process behind self-assembly and self-organization of molecules is crucial for industry. Most if not all products in food, pharmaceutical, personal and health care industries either contain surfactants or are produced by using surfactants, which are prone to self-assembly. Moreover, self-assembled surfactant mesophases are widely used as templates in the synthesis of advanced nanomaterials, such as nanoporous adsorbents, catalysts, and drug delivery vehicles.

The ability to predict mesoscale self-assembly and transport properties in complex multicomponent systems, which depend on the chemical structure of system components, is a critical step in developing new surfactant formulations for materials with improved properties. There is a fundamental gap between qualitative understanding of self-assembly in mixtures of amphiphilic molecules and its quantitative description for the systems of given chemical structure. This gap is related with the multiscale nature of self-assembly and the necessity of using coarse-grained simulation methods, which require a unified, straightforward and computationally inexpensive approach to parameterization and validation of interaction potentials.

DPD simulations[2] have been widely used in modelling soft matters over decades according to its advantages of reaching longer time scale and larger space scale. In DPD simulations, the molecule is commonly dissected into fragments of approximately equal volume, according to the number of water molecules. Those quasi particles are always called beads and interact with pair-wise force. This simple

model provides significant computational efficiency. Besides the traditional applications to self-assembled non-ionic soft structures (such as micellar solutions, block copolymers, lipid bilayers),[3-8] soft-core modeling has been recently extended to more complex systems where long-range electrostatic interactions play a key role.

The first attempts involved no explicit long-range electrostatics but effectively replaced them by short-range interactions.[9] This approach was applied not only in DPD, but also in mesoscale dynamic DFT[10].

Introduction of smeared charge model by Groot[11] enabled explicit charge simulations. Instead of point charge model standard in molecular dynamics (MD), the charge is modeled as charge cloud around the bead center using a charge density distribution function. Linear,[11] exponential,[12] Gaussian-type[13] and Bessel-type[14] decay of charge density have been attempted in the literature.[11, 12, 15-19] Actually, the charge distributions are artificial. Warren and Vlassov[14] advice choosing the distribution type and parameters to max the computational efficiency rather than to match particular thermodynamic or structural properties. Indeed, the influence of charge distribution on thermodynamics and structure of electrolytes haven't been examined carefully yet. Furthermore, even qualitative behavior of smearing charge theory in DPD simulation has not been tested. All smeared charge models consider isotropic, spherically symmetric charge distribution that rarely correspond to the actual structure of complex cations or anions in ionic surfactants and polyelectrolytes. Secondly, the charges interact in isotropic medium characterized by a constant dielectric constant ε, which means that local environment does not influence electrostatic interactions between two charges.

In this work, we examine the capability of smearing charge theory through DPD methodology. As a test system, we use micellization in two common surfactants:

sodium dodecyl sulfate (SDS, Figure 1a) and cetyl trimethyl ammonium bromide (CTAB, Figure 1b) as well as their mixtures. We target critical micelle concentration (CMC), aggregation number (N_{ag}), their dependence on the concentration of added electrolyte and difference in the structures of single-component surfactants and surfactant mixtures. The methodology and results described in Chapter 2 have been published as "Modeling Aggregation of Ionic Surfactants Using a Smeared Charge Approximation in Dissipative Particle Dynamics Simulations".[1] We also design the coarse-grained model for carbopol system with similar systematic methodology. The stability of carbopol film have been tested in aqueous solution.

Chapter 2 Ionic Surfactant

2.1 Simulation Details

2.1.1 Coarse-grained model and force between coarse-grained particles

We consider two ionic surfactants in our study: anionic surfactant Sodium dodecyl sulfate (SDS) and cationic surfactant Cetyl trimethyl ammonium bromide (CTAB). In this work, we use coarse-grained model to describe our ionic surfactants. Following the general DPD methodology,[20] the surfactants are dissected into hydrophobic tail T beads and charged hydrophilic head H beads corresponding to same size of water W beads that represent N_w=4 water molecules per bead. Counterions are represented by C/A beads. For each SDS surfactant, it is dissected into three tail beads (-$CH_2CH_2CH_2CH_2$-) and one anionic head bead (-OSO_3-). CTAB is dissected into four tail beads and one cationic head bead (-$NCH_3CH_3CH_3$-). For each charged headgroup, it is neutralized by a single monovalent counterions according to its headgroup type. The coarse-grained models for SDS and CTAB are presented in Figure 1.

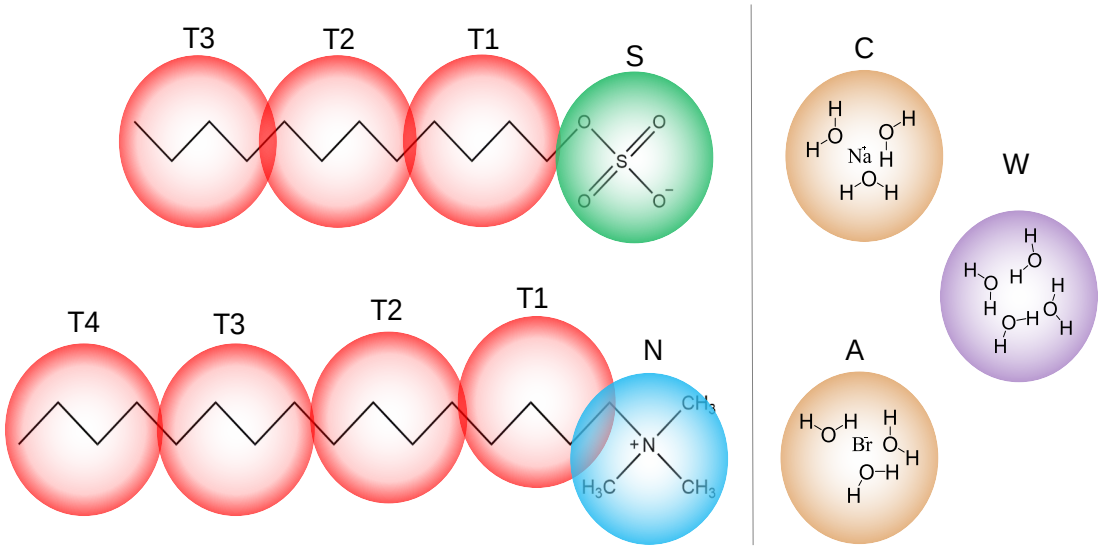

Figure 1. Schematic of coarse-grained model of SDS and CTAB molecule. SDS is coarse-grained as 3 tail T bead and one head S bead while CTAB is represented as 4 tail bead and one head N bead. Counter ions are represented as C and A bead. Water is represented as W bead.

In a standard DPD simulation, [20] the movement of bead is governed via pairwise interaction, including conservative soft repulsive, random, drag, bond, and electrostatic forces.

$$\mathbf{F}_{ij}(\mathbf{r}_{ij}) = \mathbf{F}_{ij}^{(\mathrm{C})}(\mathbf{r}_{ij}) + \mathbf{F}_{ij}^{(\mathrm{B})}(\mathbf{r}_{ij}) + \mathbf{F}_{ij}^{(\mathrm{E})}(\mathbf{r}_{ij}) + \mathbf{F}_{ij}^{(\mathrm{R})}(\mathbf{r}_{ij}) + \mathbf{F}_{ij}^{(D)}(\mathbf{r}_{ij}, \mathbf{v}_{ij}) \qquad (1)$$

All beads are assigned an equal effective diameter R_c. The soft repulsion force $\mathbf{F}_{ij}^{(\mathrm{C})}$ acts between overlapping beads: $\mathbf{F}_{ij}^{(\mathrm{C})}(\mathbf{r}_{ij}) = a_{IJ}(1 - r_{ij}/R_c)\mathbf{r}_{ij}/r_{ij}$ at $r < R_c$, $\mathbf{F}_{ij}^{(\mathrm{C})}(\mathbf{r}_{ij}) = 0$ at $r \geq R_c$, where a_{IJ} is the repulsion parameter specific to the given bead pair of types I and J. Following the standard approach to DPD simulations of self-assembly, [8] the intra-component repulsion parameters a_{II} between beads of the same type are set equal, irrespective to the bead type. The beads are tightly packed with a substantial overlap. We accepted the reduced bead packing density of ρR_c^3=3, common in DPD simulations. [8]

The random and drag force also acted between overlapping beads along the line connecting the bead centers. Random force $\mathbf{F}_{ij}^{(R)}$ that accounts for thermal fluctuations, is taken proportional to the conservative force that is also acting along the vector between the bead centers: $\boldsymbol{F}_{ij}^{(R)}(r_{ij}) = \sigma w^{R} r_{ij} \theta_{ij}(t) \mathbf{r}_{ij}$, where $\theta_{ij}(t)$ is a randomly fluctuating in time variable with Gaussian statistics. The drag force is velocity-dependent: $\boldsymbol{F}_{ij}^{(D)}(\mathbf{r}_{ij}, \mathbf{v}_{ij}) = -\gamma w^{D}(r_{ij}) (\mathbf{r}_{ij} * \mathbf{v}_{ij})$, where, $\mathbf{v}_{ij} = \mathbf{v}_j - \mathbf{v}_i$, $\mathbf{v}_i$ and $\mathbf{v}_j$ are the current velocities of the particles. We assume the common relationship between the drag and random force parameters $w^{D}(r) = [w^{R}(r)]^2 = (1 - r/R_c)^2$ at $r < R_c$, $w^{D}(r) = 0$ at $r \geq R_c$. σ and γ are parameters that determine the level of energy fluctuation and dissipation; they are related as $\sigma^2 = 2\gamma kT$ that allows to maintain constant temperature in the course of simulation via the Langevin thermostat. We assumed $\gamma = 4.5$, a common value fitted to the diffusion coefficient of water.

Intramolecular forces are introduced by binding beads together into a chain. To describe the molecule structure, the neighboring beads and second neighbor beads are connected by FENE bond force $\mathbf{F}_{ij}^{(B)}(\mathbf{r}_{ij}) = k_b(r_0 - r_{ij})/(1 - ((r_{ij} - r_0)^2/r_m^2))\mathbf{r}_{ij}/r_{ij}$,where K_b is bond rigidity, r_0 is the equilibrium bond length, and r_m is the maximum bond length. Following our recent papers. [21-23] In addition to this nearest neighbor (1-2) bond, we also take into account the second neighbor (1-3) bonds in order to control the skeleton rigidity and sidechain flexibility.

Long-range electrostatic force $F_{ij}^{(E)}$ has also been applied through smearing charge theory. The electrostatic interactions are modeled using the smeared charge approach with the exponential charge density distribution, in order to remove the divergency when $r_{ij} \rightarrow 0$. [12] $f(r) = \frac{q}{\pi\lambda^3} \exp\left(-\frac{2r}{\lambda}\right)$, where λ is smear length. The electrostatic

force $\mathbf{F}_{ij}^{(E)}$ between charged particles i and j in eq. 1 is expressed as

$$\mathbf{F}_{ij}^{(E)}(\mathbf{r}_{ij}) = \frac{e^2 q_i q_j}{4\pi kT\varepsilon_0\varepsilon_r R_C r_{ij}^2}\left[1-\exp\left(-2R_C r_{ij}/\lambda r_{ij}\right)\left(1+2R_C r_{ij}/\lambda\left(1+R_C r_{ij}/\lambda\right)\right)\right]\frac{\mathbf{r}_{ij}}{r_{ij}}.$$

2.1.2 Parameterization of the DPD model.

Following the conventional DPD setting, the intracomponent repulsion parameter is set equal for all bead types $a_{WW} = a_{TT} = a_{HH} = a_{CC} = 106.5k_BT/R_c$, which is directly determined from water compressibility. [18] The repulsion parameters intercomponent interactions and bond parameters are estimated by the fitting to MD simulation. [24] We performed MD simulations of pure hexadecane polymer melt. The MD trajectories of MD simulation were saved. Each hexadecane molecule was dissected into 4 fragments. Each fragment contain 4 CHx group. The probability distributions of distances between the centers of mass of each fragments were calculated. After that, we performed DPD simulations at similar conditions and fitted the nearest neighbor and second neighbor bond parameter to the MD distance distribution figure. The results are shown in Figure 2. Our model is capable to reproduce accurately the rigidity of the hexadecane polymer chain by only applying 1-2 and 1-3 bonds. The resulting parameters are given in Table 1.

On the next step, we evaluate parameter a_{WT} for short-range repulsion between T and W beads from the solubilities of octane in water and water in octane following our recent work. [21] Octane molecule is presented as a T-T dimer. a_{WT} is estimated from the best match between the solubility of DPD model of octane in DPD water bath and the experimental solubility. The dependence of the solubility on a_{WT} is obtained using the standard Widom test particle method [25]. The procedure was repeated for water solubility in octane and the resulting a_{WT} values are averaged. In the latter simulation,

the bead density in the system was 3.05 in order to equalize the pressures in water and octane baths. The resulting $a_{WT} = 129.9\ k_BT/R_c$.

The surfactant heads are assumed hydrophilic $a_{WS} = a_{WN} = a_{SN} = 106.5\ k_BT/R_c$, $a_{TS} = 136.5\ k_BT/R_c$ and $a_{TN} = 111.5\ k_BT/R_c$. The parameters for 1-2 and 1-3 bonds between head and tail beads were estimated similarly to those for T-T bonds. We simulated dilute aqueous solutions of SDS and CTAB in atomistic MD simulations and fitted the DPD parameters to MD results (Figure 3). DPD simulation showed a very good match to the MD configurations. All bonded and non-bonded parameters are given in Table 1.

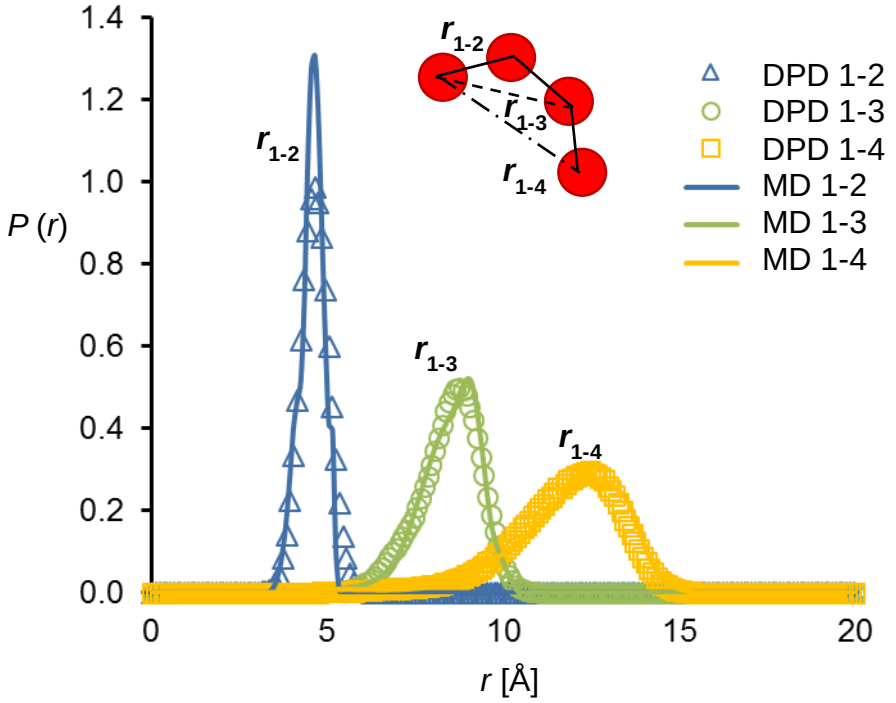

Figure 2. Bond rigidity fitting from DPD model of pure hexadecane $C_{16}H_{34}$ to the results of atomistic MD simulations at T = 298 *K*. The solid lines are obtained by MD simulations and open symbols by DPD simulations. The distribution of distances between the chain DPD beads separated by one (1-2), two (1-3) and three (1-4) nearest-neighbor FENE bonds are matched to the distributions of distances between the centers of mass of the corresponding fragments of the atomistic chain, each of which contains four CH_3 or CH_2 groups.

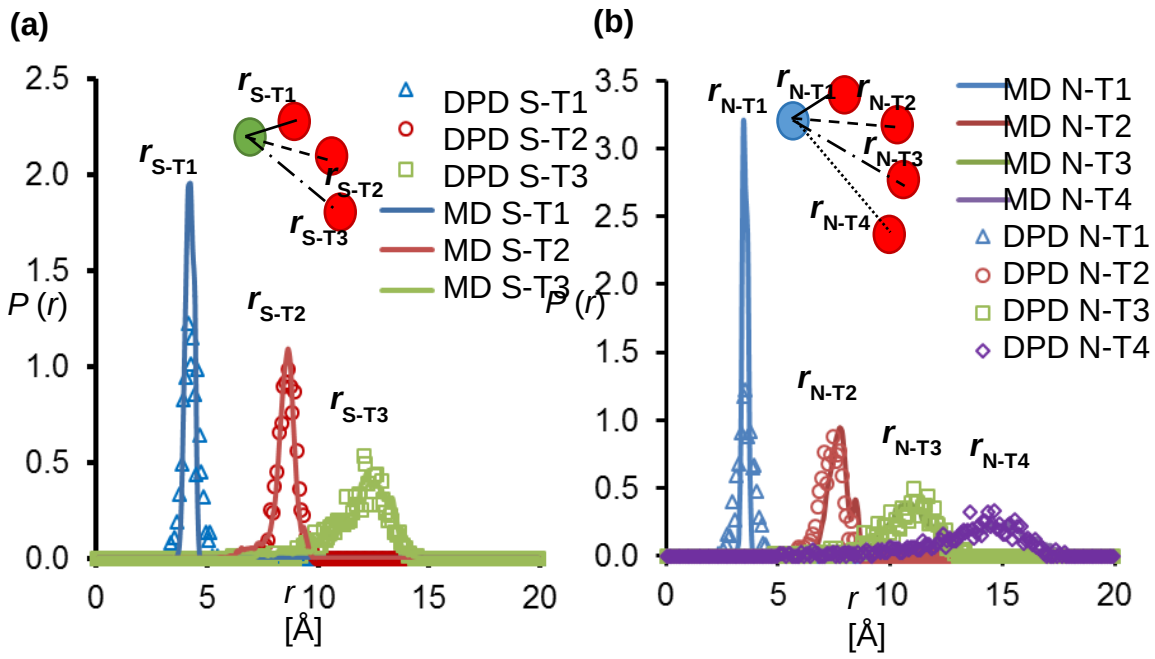

Figure 3. Fitting the parameters for head – tail bonds S-T1, S-T2, N-T1 and N-T2 in the DPD model to the results of atomistic MD simulations of SDS and CTAB in dilute aqueous solution at T = 298 *K*. The bead denotations correspond to Figure 1. DPD distributions of distances between the beads are matched to the distributions of distances between the centers of mass of the corresponding fragments (Figure 1). The solid lines are obtained by MD simulations and open symbols by DPD simulations.

Table 1. Repulsion and bond parameters of the DPD model. Short-range repulsion parameters a_{IJ} are given in k_BT/R_c units.

Repulsion parameters							
Bead type	Fragment	W	T	S	N	C^+	A^-
W	$4H_2O$	106.5					
T	$(CH_x)_4$	129.9	106.5				
S	$-OSO_3^-$	106.5	136.5	106.5			
N	$-N(CH_3)_3^+$	106.5	111.5	106.5	106.5		
C^+	$Na(H_2O)_3^+$	106.5	129.9	106.5	106.5	106.5	
A^-	$Cl/Br(H_2O)_3^-$	106.5	129.9	106.5	106.5	106.5	106.5
Bond parameters							
Bond type	Bead types	K_b/k_T		r_0/R_c		r_m/R_c	
1-2	T-T	280		0.605		2.0	
	T1-S	300		0.5		∞	(a)
	T1-N	200		0.4		∞	(a)
1-3	T-(T)-T	20		1.5		4.0	
	T2-(T1)-N	150		1.3		∞	(a)
	T2-(T1)-S	120		1.1		∞	(a)

* (a) harmonic bond

DL_MESO package [26] is employed for the DPD simulations of micellization. All simulations are performed in periodic cubic boxes, varying from 30 to 40R_c. The surfactant volume fraction ϕ is varied from 0.02 to 0.08. For all simulations, the time step δt was set equal to 0.02 and the friction parameter γ is set to 4.5 in order to keep temperature deviation under 1%. The length of each simulation was 2 million steps,

half of that was discarded for equilibration. Configurations are dumped to trajectory file every 2000 steps after equilibrium for analysis. Visualization of all molecular configurations is generated by VMD.

2.2 Results and discussion

2.2.1 Critical micelle concentration

Two surfactant molecules are considered to belong to the same aggregate if any two of their tail or middle beads overlap. If an aggregate contains more than a certain threshold n_{mic} of surfactant molecules, it was counted as a micelle. If a surfactant molecule belonged to a cluster containing less than n_{mono} surfactant molecules, it is assumed to belong to the aqueous solution of monomers in equilibrium with the micelles and is treated as "the free surfactant". Aggregation is considered as complete and equilibrium reached when the CMC and micelle numbers stabilizes and becomes practically insensitive to the choice of n_{mono} and n_{mic} within reasonable limits. [21]

Figure 4 shows the probability of a surfactant molecule to belong to an aggregate of a particular size in CTAB and SDS in aqueous solution at different concentration. It appears that at $\phi = 0.02$ characterizing of aggregation is very difficult since there is no clear difference between the free surfactant and micelles, which is probably related to insufficient systems size. However, this difference is very clear for higher concentrations. We therefore use $n_{mono}= 5$ and $n_{mic}=20$ for SDS and $n_{mono}= 3$ and $n_{mic}=8$ for CTAB in order to calculate the free surfactant concentration and the micelle size. The dependence of the free surfactant concentration ϕ_f on ϕ is shown in Figure 5. It is clear that ϕ_f actually decreases as ϕ increases. This differentiates the behavior of ionic surfactants from that on non-ionic ones, where ϕ_f slowly increases with ϕ and can be with a very reasonable precision assumed as CMC. Below CMC,

$\phi = \phi_f$. Formation of micelles actually leads to a decrease in free surfactant concentration in the surrounding solution. This behavior results from the electrostatic interactions between the micelles and surrounding surfactant and is specific to ionic surfactants. This behavior of ionic surfactant was observed experimentally, [27, 28] predicted theoretically [29, 30] and by MC simulations [31] and is correctly reproduced with the smeared charge model in DPD. For non-ionic surfactants, ϕ_f slowly increases with ϕ and can be with a very reasonable precision assumed as CMC.[21]

In order to calculate the CMC from ϕ_f and ϕ, we employed a semi-empirical theory of Sanders et al, [29, 30] which relates the free surfactant concentration C_f and total surfactant concentration C_T as:

$$\log(C_f) = (1+\alpha)\log(C_{CMC}) - \alpha\log\left(\frac{(1-\alpha)(C_T - C_f) + C_f}{1 - VC_T}\right) \qquad (2)$$

where V is the molar volume of surfactant and C_T, C_f and C_{CMC} are expressed in mol/L. α is the degree of association of the counterions with the head groups for the surfactants forming the micelles.

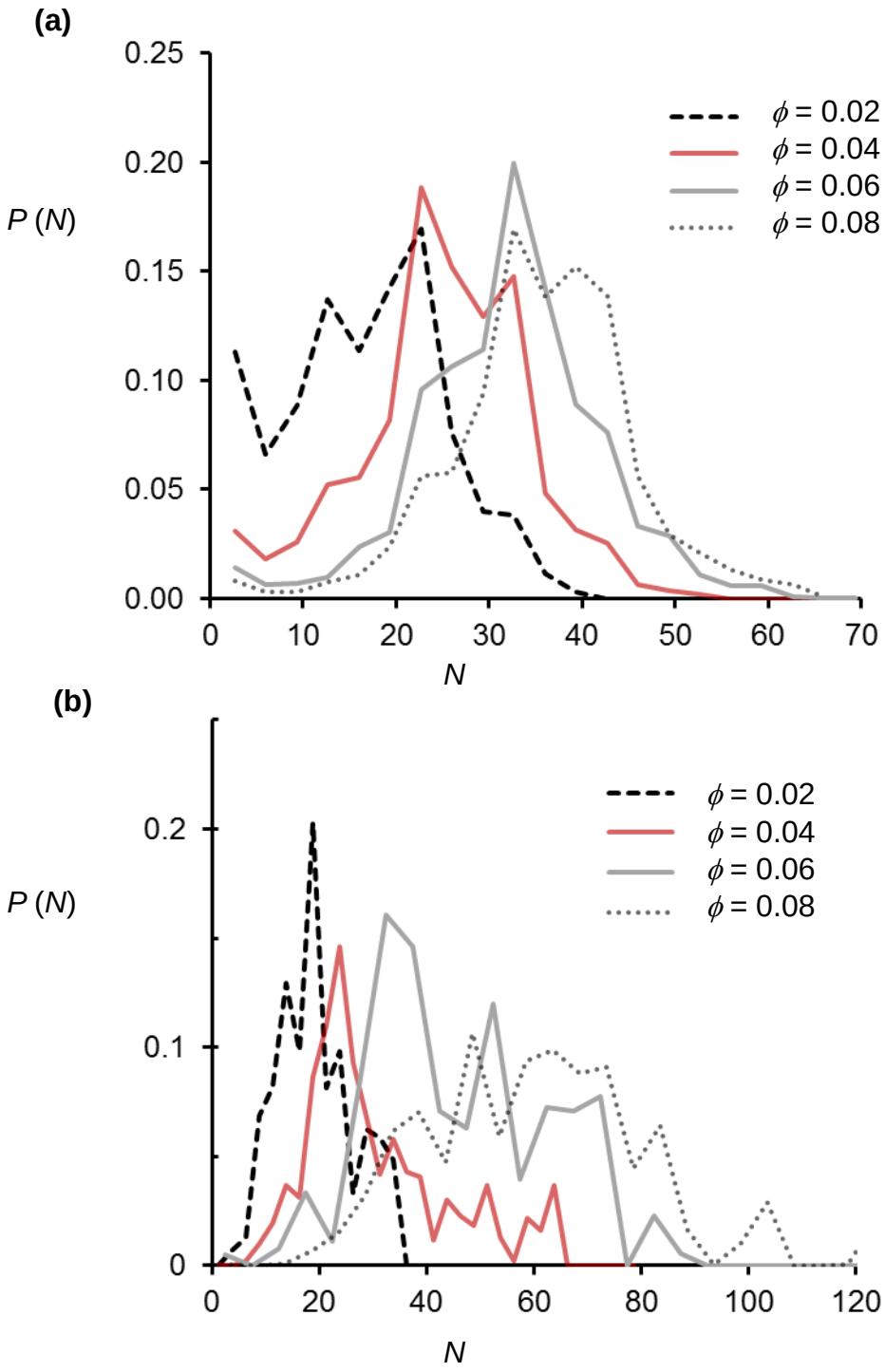

Figure 4. Probability distribution of finding a surfactant molecule in an aggregate consisting of N molecules for (a) SDS and (b) CTAB at different overall surfactant volume fractions.

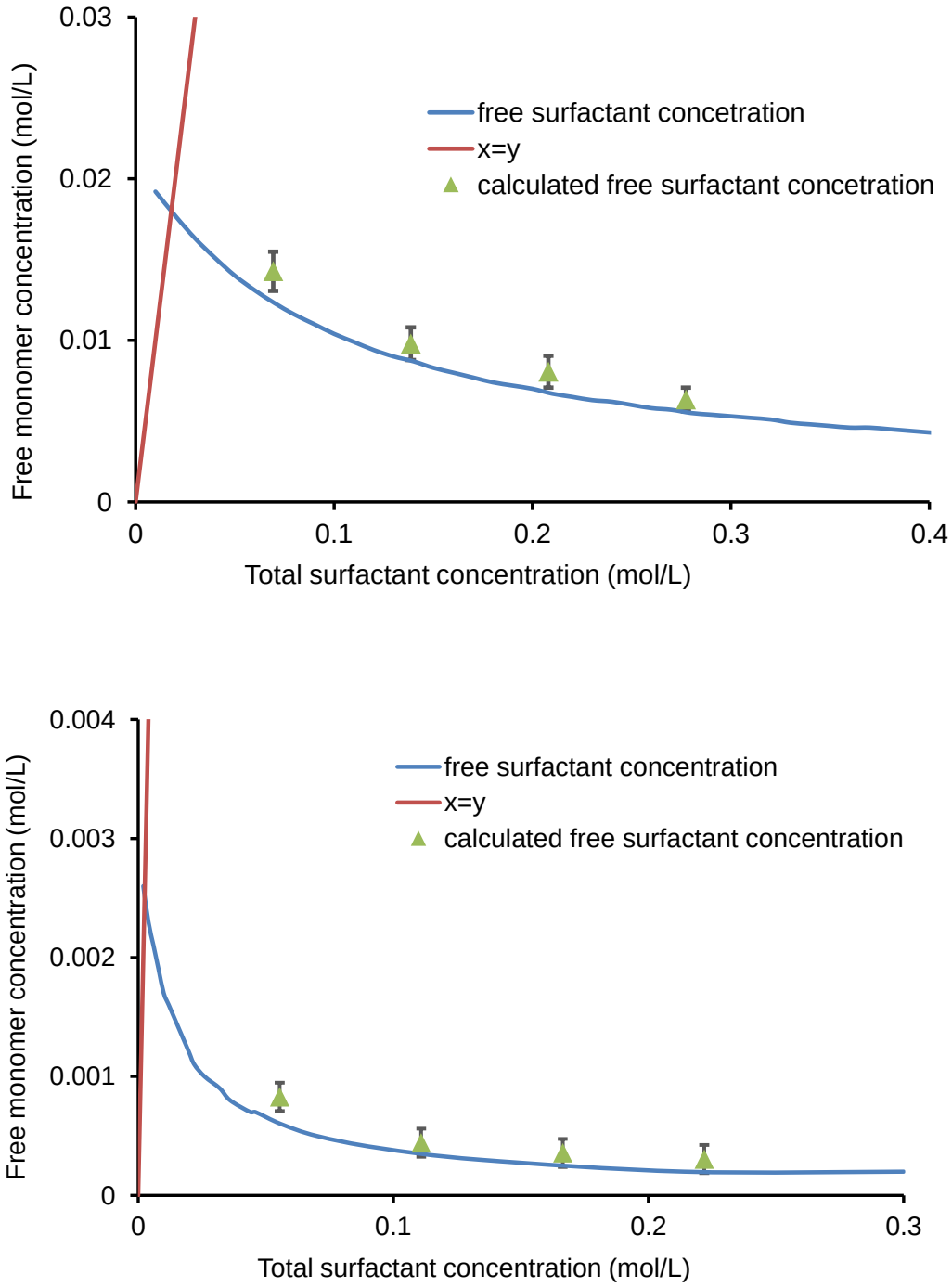

Figure 5. (a) Obtained CMC of SDS from eq. (2). (b) CMC of CTAB obtained from eq. (2). The blue line is the free surfactant concentration mf obtained from eq. (3). The red line is the relationship "x=y". The green triangles are calculated free surfactant concentration obtained from simulations at different surfactant volume

fraction. The intersection of red line and blue line is the obtained CMC of SDS and CTAB.

Figure 5 shows the obtained CMC of SDS and CTAB in aqueous system. The obtained CMC of SDS system is 18mM while the experimental data is 8mM[32]. The obtained CMC of CTAB system is 2.4mM and the experimental data is 0.9mM[32]. The free monomer concentration calculated from The CMCs of these two surfactant systems are around 2 times greater than experimental data, but are still in the reasonable range. This inaccuracy can be explained as lack of parameterization method for head and water groups. Micellization of ionic surfactant is not only controlled by hydrophobic effect, but also affected by hydrophilic interaction between charged group and water. The repulsion parameters between head and water may be too strong, which hindered the process of micellization and raised CMC. Overall, CMCs calculated from the free monomer concentration of these two surfactant systems are around 2 to 3 times greater than experimental data, but are still in the reasonable range.

2.2.2 Micelle sizes

In the next step, we evaluate the micelle size of pure surfactant system. The aggregation number obtained from simulations various with the surfactant volume fraction at different surfactant systems. It tend to aggregates into larger micelle with the total surfactant loading of SDS and CTAB. The trend of increased aggregation number is found to be consistent with the tendency determined from experimental data[32], but the aggregation number itself is found to be lower than the experimental value. The aggregation number of CTAB is slightly larger than SDS surfactants. The larger aggregates for CTAB surfactants can be explained as the fact that CTAB

molecule is longer and its micelle surface area is greater than SDS so that it can accommodate more head groups.

The geometrical analysis and probability distributions given in Figure 4 also allows evaluation of micelle sizes. From the distributions, we calculated aggregation number N_{ag} (that is the average number of surfactant molecules in a micelle). The micelles grow with the total surfactant concentration, which is a well-establishes tendency in surfactant solutions. It should also be noted that experimental N_{ag} for the same systems vary with the method used. [29, 33, 34] But in general, it is obvious that our micelles are much (2-3 times) smaller than the experimentally observed sizes. For example, the experimental aggregation number at 50mM SDS is around 65 while we obtained value is around 30 at ϕ=0.04, which approximately corresponds to 0.14M. The aggregation number of CTAB calculated from simulation is larger than SDS surfactants. This is natural and consistent with the experimental results, for CTAB molecule is longer and its micelle surface area is greater than SDS so that it can accommodate more head groups.

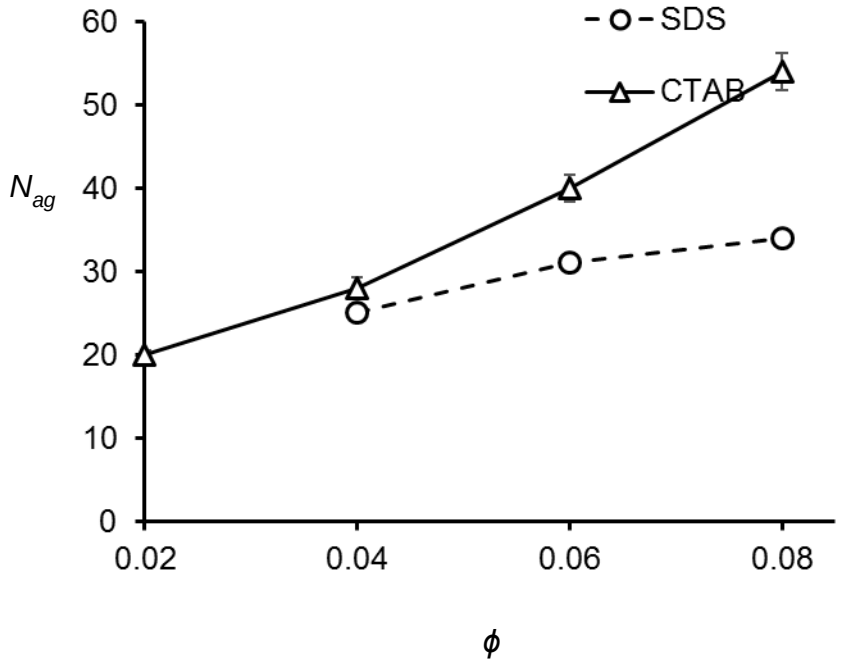

Figure 6. Dependence of aggregation number on surfactant volume fraction for SDS and CTAB. The system size is $40\times40\times40R_c^3$.

2.2.3 Salt effect

The properties of SDS aggregates in saline solution at the presence of sodium chloride (NaCl) has been studied through DPD approach as well. Fixed SDS volume fraction ϕ=0.04 has been chosen at box L=30Rc. A series simulation has been performed by gradually adding 1:1 electrolyte solution C^+A^-, approximately regarded as salt, from 0.5M to 2M into this system.

As the concentration of added salt increases, the micelle structure and morphology between micelle and free surfactants changes as well. At salt free systems, both SDS and CTAB surfactants self-assembled toward spherical micelles and the spherical aggregates remains until 0.5M salt added. Rodlike micelles have initially been observed at the system under 1M salt. With the continually increased total salt loading, rodlike micelles aggregate into larger size and form longer micelles. At the meantime, less free surfactants can be detected from the systems. The transition from spherical micelle to rodlike shape have been inspected from snapshots obtained by simulations from C_{salt}=0.5M to C_{salt}=1M. This potentially sphere to rod transition has also been detected from experiments around C_{salt}=0.6M [35, 36]. This good agreement with experiments proof the capability of DPD approach that can mimic more complicated long-range electrostatic interaction between anionic surfactant and salt through smearing charge theory. Although our simulation shows the limitation of predict aggregates size, the main sphere-rod transition and larger aggregates tendency have been captured from these simulations.

Figure 7 shows the snapshots of SDS at different additional salt concentrations after equilibrium. The micelle size distribution clearly changes along with the distribution of the asphericity factor, a generalized quantitative measure of the departure from spherical symmetry of micelles.[37] The asphericity factor A is obtained from the gyration tensor S calculated for each individual micelle: $S_{ij} = 1/N \sum_{l=1}^{N} \left(S_{il} - S_i^{\mathrm{CM}}\right)\left(S_{jl} - S_j^{\mathrm{CM}}\right)$, where S_i^{CM} stands for the center of mass coordinate (i denotes x, y, or z). After three eigenvalues R_1^2, R_2^2, R_3^2 of the gyration tensor are obtained, the asphericity factor is calculated as $A = 1/2R_{\mathrm{g}}^4 \left[\left(R_1^2 - R_2^2\right) + \left(R_1^2 - R_3^2\right) + \left(R_3^2 - R_2^2\right)\right]$, where $R_{\mathrm{g}}^2 = R_1^2 + R_2^2 + R_3^2$ is the radius of gyration. The asphericity factor is 0 for perfectly spherical micelles and reaches 1 for perfect cylinders. It is clear that the addition of salt sharply decreases the fraction of spherical micelles increases the number of elongated micelles at 0.5M and 1M added electrolyte concentrations. In 2M electrolyte solution, the asphericity distributions show a well-defined peak corresponding to cylindrical micelles.

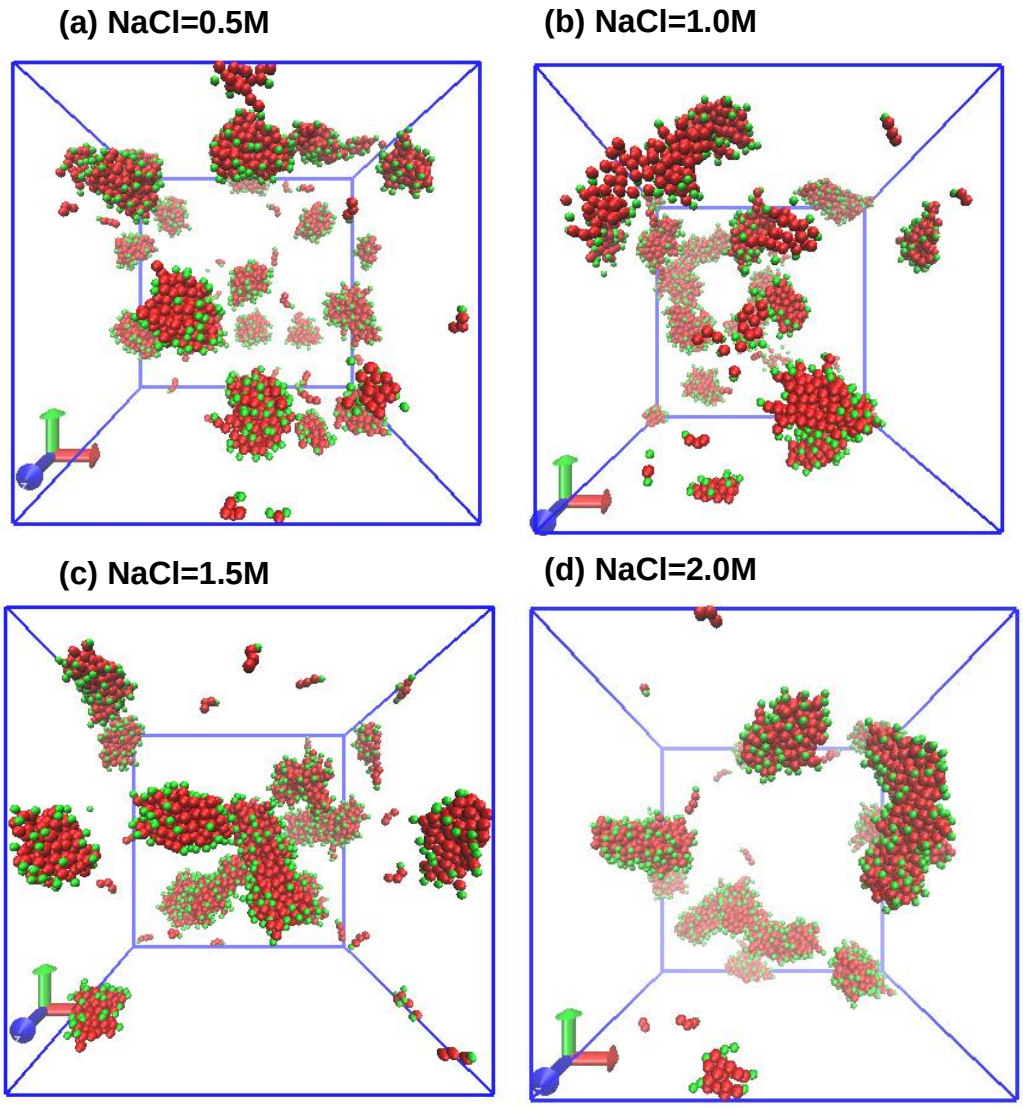

Figure 7. Final configuration of SDS at presence of NaCl. (a) NaCl=0.5 M (b) NaCl=1M (c) NaCl=1.5M (d) NaCl=2M. The red beads are tail beads and green beads are head beads of SDS surfactants.

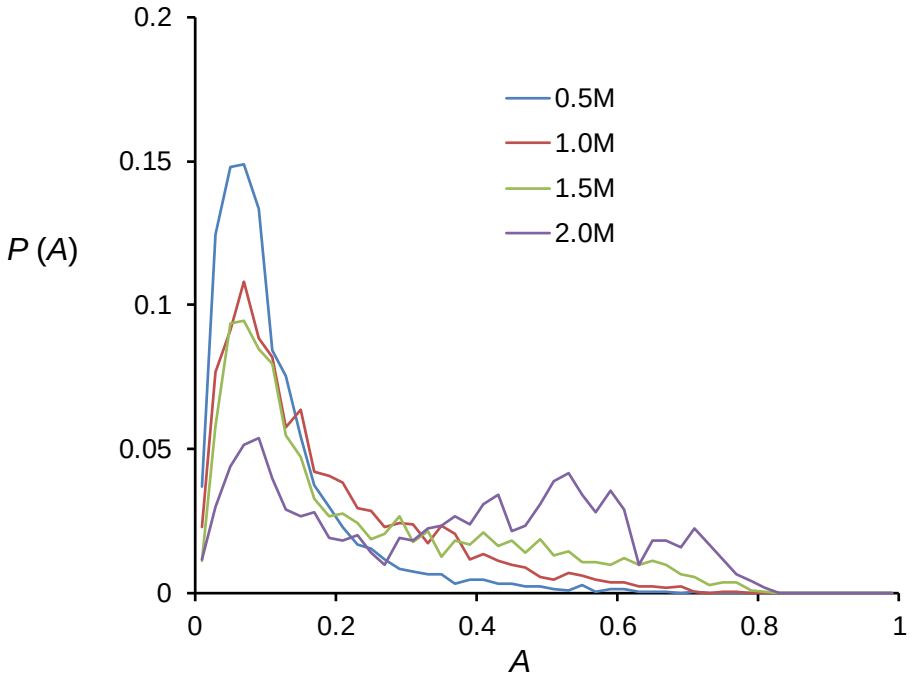

Figure 8. Distribution of asphericity factors of SDS micelles at different salt concentrations. A=0 corresponds to the spherical micelle shape; larger values of A characterize aggregates of elongated shape.

2.2.4 Mixtures of cationic and anionic surfactants.

Mixtures of cationic and anionic surfactants provide another qualitative test for smeared charge models. When a surfactant with a different charge of the head group incorporates into the micelles, the overall charge of the micelles surface layer decreases, a corresponding decrease of the chemical potential of surfactants in the micelles causes reduction in free surfactant concentration (which means lower CMC) and growth of micelle size. As introduce of oppositely charged surfactant, initially spherical micelles adopt a worm-like shape and then elongate into uni-lamella vesicles. For the particular system considered here, the transition to a vesicular structure for SDS-rich mixtures is achieved at 35:65 ratio between CTAB and SDS molarities.

We perform simulations of SDS-CTAB mixtures at constant ϕ=0.08. The SDS/CTAB molar ratio was varied. We consider 9/1, 2/1, and 1/1 SDS-CTAB mixtures in aqueous solution. Figure 8 shows a snapshot of surfactant configuration for 9/1 SDS/CTAB mixture. When additional CTAB is added into the system, the micelles start to elongate and adopt a worm-like shape. As the SDS/CTAB ratio changes to 2/1, the morphology drastically changes. Rather than cylindrical micelle, we observed a roughly spherical micro-vesicles. The inner part also contained certain amount solvent. Interestingly enough, the micro-vesicles never merge or form a single bilayer. If the surfactant ratio of CTAB is continually raised to 1/1 ratio, the micro-vesicles merge and a phase separation occurs, which shows an irregular structure. Note that the soft-core model does not allow for a formation of a crystalline surfactant phase. Overall, in general the model does reproduce the general features of the phenomenon, but also shows substantial quantitative deviations from the experimental behavior. We also observed that although a_{HW} barely affect CMC, it has substantial influence on the segregation morphology changes as the fraction of the opposite charge surfactant increases. For example, Figure 9 shows structural evolution of the same system with $a_{HW}=96.5k_BT/R_c$ (that is, head-water interactions are much more favorable, than head-head or water-water interactions). At 9/1 SDS/CTAB ratio, we observe the formation some spherical aggregates (Figure 9d). Further increase of CTAB fraction to 2/1 leads to well-defined cylindrical structure and then unilamella morphology at 1/1. This model with $a_{HW}=96.5k_BT/R_c$ seems to give a reasonable agreement with the experiment as far as the morphology evolution is concerned. However, the absence of methods for rigorous derivation of the parameters between charged species makes conclusion of agreement of DPD and experiment very difficult. This suggest a further development of parameterization method for charged head group in DPD simulations.

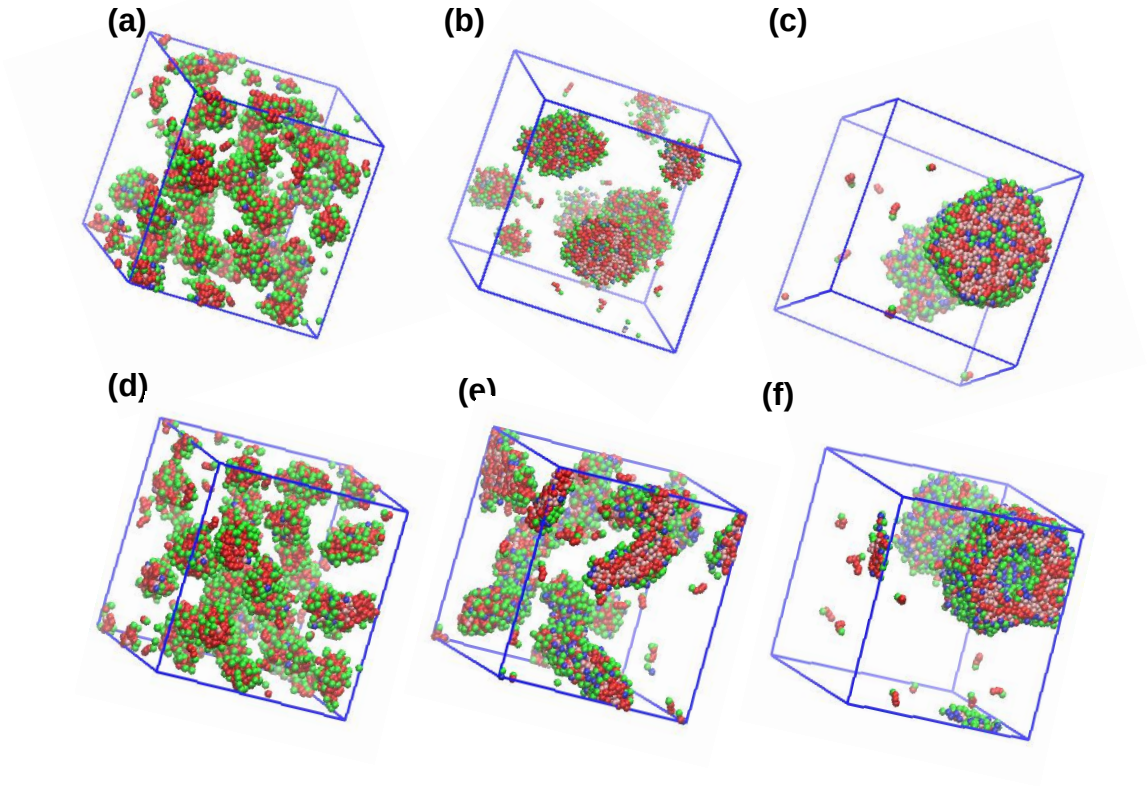

Figure 9. Final configuration of catanionic mixture at different ratio (total surfactant volume fraction ϕ_{total}=0.08) under different head-water repulsion. (a-c) with $a_{HW}=106.5k_BT/R_c$ (d-e) with $a_{HW}=96.5k_BT/R_c$. (a) & (d) The snapshots of 9/1 SDS-CTAB mixture. (b) & (e) The snapshots of 2/1 SDS-CTAB mixture. (c) & (f) The snapshots of 1/1 SDS-CTAB mixture. The red beads and pink beads are SDS and CTAB tail beads while green beads and blue beads are SDS and CTAB head beads separately.

Chapter 3 Carbopol

3.1 simulation details

3.1.1 Coarse-grained model

Following the general DPD methodology, we extended our methodology to carbopol system. Here we dissect the carbopol into beads of approximately similar size following the former procedure: hydrophobic side chain T beads and hydrophilic skeleton chain P and M beads as shown in Figure 10. Water is modelled with W beads, and each W bead contains 4 water molecules. Each T bead equals four methyl/methylene groups of the alkyl chain. [21] Each skeleton P and M bead contains -$CH_2CHCOOH$- group. P bead is the skeleton bead while M bead is the connection bead between side chain and skeleton chain.

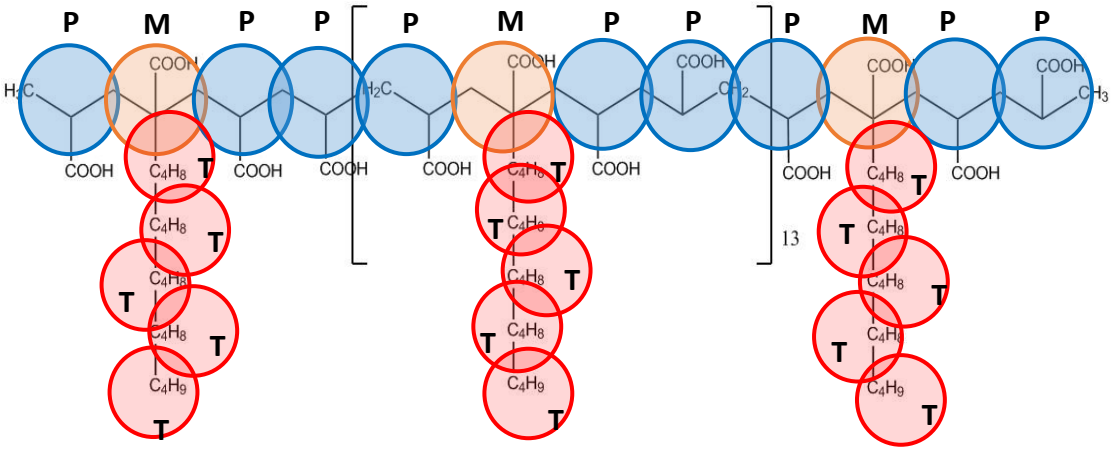

Figure 10. Schematic of coarse grained model of carbopol. Carbopol is represented as polyacrylic acid skeleton chain by P and M beads. The side chain is represented by 5 tail T beads.

3.1.2 Parameterization method for DPD model

Following the standard DPD implementation, the intracomponent repulsion parameter is the same for all bead types $a_{WW} = a_{TT} = a_{PP} = a_{MM} = 106.5k_BT/R_c$ and is determined from water compressibility same as chapter 2. [18] The intercomponent repulsion parameters between butane and water is $a_{WT}=129.9k_BT/R_c$, which is same as chapter 2. One the next step, we evaluate other intercomponent repulsion parameters following the similar method as our recent work. [21]The reference compound and repulsion parameter are listed in Figure 11 and Table 2. The reference compound for connection bead M is Methyl Acetate due to its increased hydrophobicity while it is connected with hydrophobic T bead.

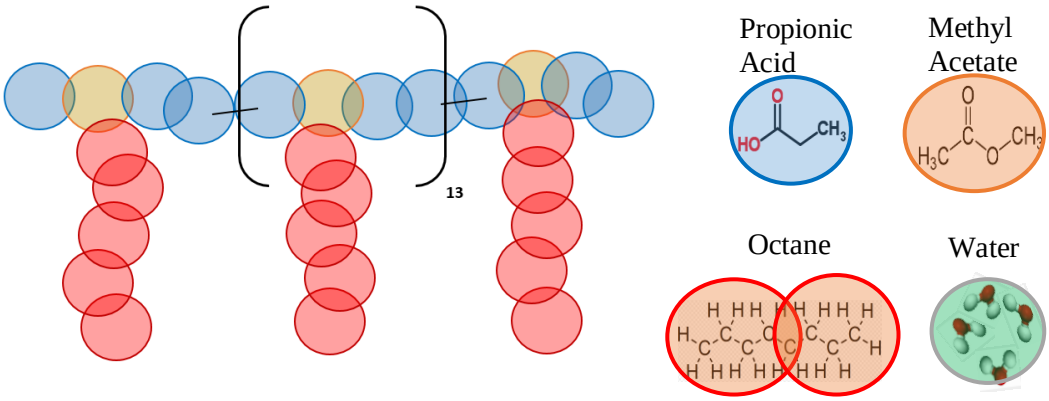

Figure 11. Schematic of reference compound. The reference compound for skeleton P bead is propionic acid while the connection M bead is Methyl Acetate. The reference compound for side chain C bead is octane dimer. Each water bead contain 4 water molecules.

Table 2. Repulsion parameters for different bead type of Carbopol. Short-range repulsion parameters a_{IJ} are given in k_BT/R_c units.

Bead type	Fragment	W	P	M	T
W	$4H_2O$	106.5			
P	$-CH_2CHCOOH-$	109.3	106.5		
M	$-CH_2CHCOOH-$	110.7	102.6	106.5	
T	$(CH_x)_4$	129.9	116.8	109.5	106.5

3.1.3 Bond parameters

For parameterization of bond potentials, we use a bottom-up approach same as chapter 2. The parameters of nearest neighbor (1-2) and second neighbor (1-3) bonds are determined by fitting the radial distribution functions for the conformations of coarse-grained chains to the results of atomistic MD simulations.

The bonds between side chain T beads are same as the one used in chapter 2. For main chain, we perform MD simulation with polyacrylic acid skeleton $CH_3CH_2COOH(CH_2CH_2COOH)_8CH_2COOHCH_3$ in aqueous system. To obtain the bond parameters for main chain bead, we simulate polyacrylic acid fragments of 10 monomers using a similar procedure. The shapes of intra-molecular bead-bead distance distributions in polyacrylic acid are much more complex compared to alkanes. Small peaks on MD distributions correspond to particular preferential conformations of carboxylate chains. However, the overall rigidity of the polyacrylic acid skeleton is reproduced within reasonable accuracy as shown in Figure 12. The bonding parameters obtained with this procedure are given in Table 3.

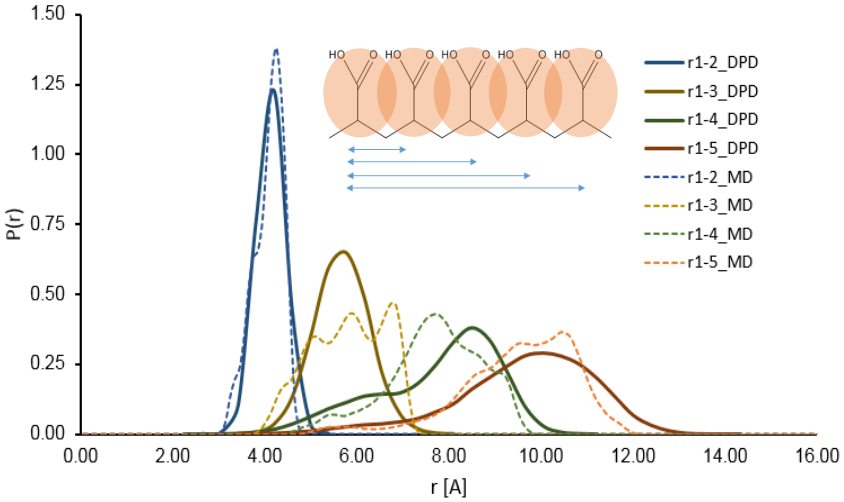

Figure 12. Fitting parameters for polyacrylic acid skeleton bonds in the DPD model to the results of atomistic MD simulations of polyacrylic acid in dilute aqueous solution. DPD distributions of distances between the beads are matched to the distributions of distances between the centers of mass of the corresponding fragments. The solid lines are obtained by DPD simulations and dash lines by MD simulations.

Table 3. Bond parameters for Carbopol.

1-2 bond				1-3 bond		
	S-S	P-S	P-P	S-S-S	S-S-P	P-P-P
K	280.00	360.00	440.00	20.00	40.00	80.00
r0	0.605	0.61	0.620	1.500	1.26	0.790
rm	2.00	2.00	2.00	4.00	3.33	2.00

3.2 Results and discussion

Using former coarse-grained model and force-field, we test the carbopol model in aqueous system with cell dimension 25x25x75, approximately 33% of which is composed of carbopol beads. After equilibrium, we observe a stable carbopol film. This model can be further used to examine the rheology of carbopol-surfactant system.

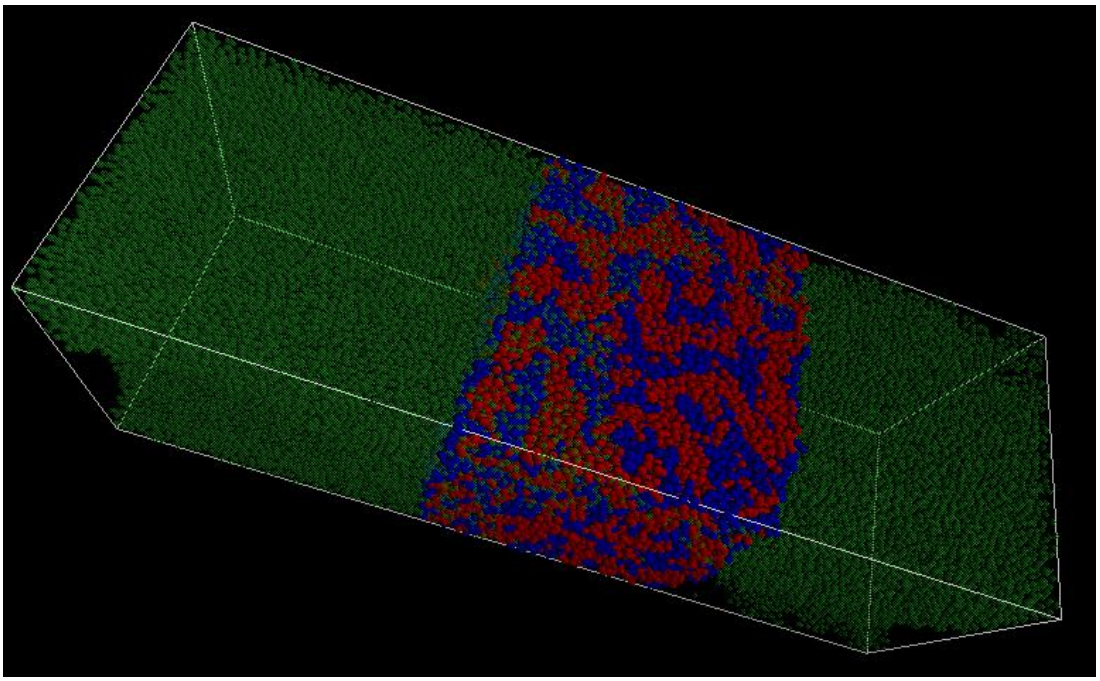

Figure 13. The snapshot of Carbopol film after equilibrium. The blue beads are skeleton beads while red one is side chain alkane bead. The transparent green bead is water bead.

Chapter 4 Conclusion

In this work, we examine the capabilities to a smeared charge model to reproduce the basic features of ionic surfactants in a standard DPD simulation. We chose a Slater-type distribution of charge around the bead center implemented in DL_MESO (to our best knowledge, currently this is the only standard DPD code where smeared charges are implements). We consider several phenomena which are unique for ionic surfactants: (1) dependence of the free surfactant concentration on the total surfactant concentration (2) the dependence of the aggregation on the concentration of added electrolyte (3) difference in the aggregation of one-component surfactant solutions and the mixtures of oppositely charged surfactants.

Overall, the model reproduces the qualitative features of ionic surfactant behavior fairly well in several different systems. The free surfactant concentration showed a decrease trend with the overall increasing total surfactant concentration after the latter has exceeded CMC, and the dependence is described well with standard semiempirical model. Despite higher than experimental CMCs that agreement between simulations and experiment is actually reasonable, considering the general accuracy of coarse-grained models in CMC prediction. An unpleasant results is a small micelle size predicted in DPD. This may be an effect of isotropic charge distribution around the ionic group and the uniform dielectric constant. The other issue is DPD model's inability to reproduce dissociation and recombination between ionic heads and counterions. Unfortunately, this problem is inherent to the smeared charge models of DPD and also to many coarse-grained forcefields and has to be taken into account when such models are employed in predictions of the behavior of electrolytes.

The effect of charge smearing achieved by addition of electrolyte is also reproduced well in DPD. The spherical micelle growth and elongation, and the transition location from spherical micelle to rod-like micelle agrees well with the experimental data. Finally, the model qualitatively describe the structure of the anionic and cationic surfactant mixtures. The simulation successfully reproduce the transition of cylindrical micelle shapes and vesicle-like aggregates and the total charge of the system decreases. The exact shape of the aggregates and conditions for the transitions between different morphologies are very sensitive to the parameters of interactions between the ionic groups and the solvent, but rigorous methods for parameterization are yet to be developed.

We also design a coarse-grained model for carbopol system, and develop relevant force-field based on our systematic methodology. The carbopol film in aqueous system is stable after equilibrium, which can be used in further investigation of the rheology carbopol-surfactant system. Further examination with additional surfactant, including both non-ionic and ionic-surfactant, are required in the future work based on this model.

REFERENCES

1. Mao, R., et al., *Modeling aggregation of ionic surfactants using a smeared charge approximation in dissipative particle dynamics simulations.* The Journal of Physical Chemistry B, 2015. **119**(35): p. 11673-11683.
2. Hoogerbrugge, P.J. and J. Koelman, *SIMULATING MICROSCOPIC HYDRODYNAMIC PHENOMENA WITH DISSIPATIVE PARTICLE DYNAMICS.* Europhysics Letters, 1992. **19**(3): p. 155-160.
3. Boek, E.S., et al., *Simulating the rheology of dense colloidal suspensions using dissipative particle dynamics.* Physical Review E, 1997. **55**(3): p. 3124-3133.
4. Groot, R.D. and T.J. Madden, *Dynamic simulation of diblock copolymer microphase separation.* Journal of Chemical Physics, 1998. **108**(20): p. 8713-8724.
5. Spenley, N.A., *Scaling laws for polymers in dissipative particle dynamics.* Europhysics Letters, 2000. **49**(4): p. 534-540.
6. Groot, R.D. and K.L. Rabone, *Mesoscopic simulation of cell membrane damage, morphology change and rupture by nonionic surfactants.* Biophysical Journal, 2001. **81**(2): p. 725-736.
7. Prinsen, P., P.B. Warren, and M.A.J. Michels, *Mesoscale simulations of surfactant dissolution and mesophase formation.* Physical Review Letters, 2002. **89**(14).
8. Groot, R.D. and P.B. Warren, *Dissipative particle dynamics: Bridging the gap between atomistic and mesoscopic simulation.* Journal of Chemical Physics, 1997. **107**(11): p. 4423-4435.
9. Dorenbos, G., *Dependence of pore morphology and diffusion on hydrophilic site distribution within hydrated amphiphilic multi block co-polymer membranes.* Polymer, 2013. **54**(18): p. 5024-5034.
10. Kyrylyuk, A.V. and J. Fraaije, *Microphase separation of weakly charged block polyelectrolyte solutions: Donnan theory for dynamic polymer morphologies.* Journal of Chemical Physics, 2004. **121**(6): p. 2806-2812.
11. Groot, R.D., *Electrostatic interactions in dissipative particle dynamics-simulation of polyelectrolytes and anionic surfactants.* Journal of Chemical Physics, 2003. **118**(24): p. 11265-11277.
12. Gonzalez-Melchor, M., et al., *Electrostatic interactions in dissipative particle dynamics using the Ewald sums.* Journal of Chemical Physics, 2006. **125**(22).
13. Warren, P.B. and A.J. Masters, *Phase behaviour and the random phase approximation for ultrasoft restricted primitive models.* J Chem Phys, 2013. **138**(7): p. 074901.
14. Warren, P.B. and A. Vlasov, *Screening properties of four mesoscale smoothed charge models, with application to dissipative particle dynamics.* J Chem Phys, 2014. **140**(8): p. 084904.
15. Posel, Z., et al., *Dissipative Particle Dynamics Study of the pH-Dependent Behavior of Poly(2-vinylpyridine)-block-poly(ethylene oxide) Diblock Copolymer in Aqueous Buffers.* Macromolecules, 2014. **47**(7): p. 2503-2514.
16. Yang, K., A. Vishnyakov, and A.V. Neimark, *Polymer Translocation through a Nanopore: DPD Study.* Journal of Physical Chemistry B, 2013. **117**(13): p. 3648-3658.
17. Wang, Y.-L., Z.-Y. Lu, and A. Laaksonen, *Specific binding structures of dendrimers on lipid bilayer membranes.* Physical Chemistry Chemical Physics, 2012. **14**(23): p. 8348-8359.
18. Vishnyakov, A., D.S. Talaga, and A.V. Neimark, *DPD Simulation of Protein Conformations: From alpha-Helices to beta-Structures.* Journal of Physical Chemistry Letters, 2012. **3**(21): p. 3081-3087.

19. Ibergay, C., P. Malfreyt, and D.J. Tildesley, *Electrostatic Interactions in Dissipative Particle Dynamics: Toward a Mesoscale Modeling of the Polyelectrolyte Brushes.* Journal of Chemical Theory and Computation, 2009. **5**(12): p. 3245-3259.
20. Groot, R.D. and P.B. Warren, *Dissipative particle dynamics: Bridging the gap between atomistic and mesoscopic simulation.* The Journal of Chemical Physics, 1997. **107**(11): p. 4423.
21. Vishnyakov, A., M.-T. Lee, and A.V. Neimark, *Prediction of the Critical Micelle Concentration of Nonionic Surfactants by Dissipative Particle Dynamics Simulations.* The Journal of Physical Chemistry Letters, 2013. **4**(5): p. 797-802.
22. Lee, M.-T., A. Vishnyakov, and A.V. Neimark, *Calculations of Critical Micelle Concentration by Dissipative Particle Dynamics Simulations: The Role of Chain Rigidity*. Journal of Physical Chemistry B, 2013. **117**(35): p. 10304-10310.
23. Vishnyakov, A. and A.V. Neimark, *Self-Assembly in Nafion Membranes upon Hydration: Water Mobility and Adsorption Isotherms.* Journal of Physical Chemistry B, 2014. **118**(38): p. 11353-11364.
24. MacKerell, A.D., N. Banavali, and N. Foloppe, *Development and current status of the CHARMM force field for nucleic acids.* Biopolymers 2001. **56**: p. 257–265.
25. Widom, B., *Some Topics in the Theory of Fluids.* J. Chem. Phys., 1963. **39**: p. 2808-2812.
26. Seaton, M.A., et al., *DL_MESO: highly scalable mesoscale simulations.* Molecular Simulation, 2013. **39**(10): p. 796-821.
27. Johnson, I., G. Olofsson, and B. Jonsson, *MICELLE FORMATION OF IONIC AMPHIPHILES - THERMOCHEMICAL TEST OF A THERMODYNAMIC MODEL.* Journal of the Chemical Society-Faraday Transactions I, 1987. **83**: p. 3331-3344.
28. Polacek, R. and U. Kaatze, *Monomer exchange kinetics, radial diffusion, and hydrocarbon chain isomerization of sodium dodecylsulfate micelles in water.* Journal of Physical Chemistry B, 2007. **111**(7): p. 1625-1631.
29. Quina, F.H., et al., *GROWTH OF SODIUM DODECYL-SULFATE MICELLES WITH DETERGENT CONCENTRATION.* Journal of Physical Chemistry, 1995. **99**(46): p. 17028-17031.
30. Sanders, S.A., M. Sammalkorpi, and A.Z. Panagiotopoulos, *Atomistic Simulations of Micellization of Sodium Hexyl, Heptyl, Octyl, and Nonyl Sulfates.* Journal of Physical Chemistry B, 2012. **116**(8): p. 2430-2437.
31. Cheong, D.W. and A.Z. Panagiotopoulos, *Monte Carlo simulations of micellization in model ionic surfactants: Application to sodium dodecyl sulfate.* Langmuir, 2006. **22**(9): p. 4076-4083.
32. Anachkov, S.E., et al., *Determination of the aggregation number and charge of ionic surfactant micelles from the stepwise thinning of foam films.* Adv Colloid Interface Sci, 2012. **183-184**: p. 55-67.
33. Weidemaier, K., H.L. Tavernier, and M.D. Fayer, *Photoinduced electron transfer on the surfaces of micelles.* Journal of Physical Chemistry B, 1997. **101**(45): p. 9352-9361.
34. Lianos, P. and R. Zana, *FLUORESCENCE PROBE STUDIES OF THE EFFECT OF CONCENTRATION ON THE STATE OF AGGREGATION OF SURFACTANTS IN AQUEOUS-SOLUTION.* Journal of Colloid and Interface Science, 1981. **84**(1): p. 100-107.
35. Berr, S.S. and R.R.M. Jones, *Effect of Added Sodium and Lithium Chlorides on Intermicellar Interactions and Micellar Size of Aqueous Dodecyl Sulfate Aggregates As Determined by Small-Angle Neutron Scattering.* 1998. **4**: p. 1247-1251.
36. Mazer, N.A., G.B. Benedek, and M.C. Carey, *An Investigation of the Micellar Phase of Sodium Dodecyl Sulfate in Aqueous Sodium Chloride Solutions Using Quasielastic Light Scattering Spectroscopy.* The Journal of Physical Chemistry, 1976. **80**(10).

37. Rudnick, J. and G. Gaspari, *The aspherity of random walks.* Journal of Physics A: Mathematical and General, 1986. **19**(4): p. L191.